

Parallel Unsteady Reynolds-Averaged Navier-Stokes (URANS) Studies of the Performance of ONR Waterjet AxWJ-2

Stephen E. Monroe 1

¹ Clarkson University, Potsdam, New York, 13699, United States

Abstract

The accuracy of SimericsMP+ Unsteady Reynolds-Averaged Navier-Stokes (URANS) is validated by studying turbulent flow past counter rotating propellers (CRPs). Subsequently, URANS is used to study an axial flow in an Office of Naval Research (ONR) waterjet and the pump's performance. Specifically, experimental data from Miller (1976) as well as LES results from Hu et al (2019) are employed to compare against the current URANS results. Due to the large size of both simulations, parallel computing over 80 cores is involved. For the CRP study, torque and thrust coefficients are plotted against a range of advance ratios, ensuring a Reynolds number of less than 500,000. For the pump, torque and head coefficients are plotted for a range of flow rates. For both studies, two different mesh sizes were utilized. The finer meshes of both studies contained roughly twice the number of cells found in their respective coarse meshes. These refinements lead to minor improvements, showing good convergence. The URANS torque and thrust coefficients were found to be within 10% of that from experimental data across all advance ratios for the CRP set, showing good agreement. The torque and head coefficients for the pump displayed even better agreement, with the greatest error across all flow conditions remaining under 3%.

Keywords: URANS, SimericsMP+, Marine Propeller, Waterjet, k-epsilon

1. Introduction

In 200 BC Greek mathematician Archimedes invented the first reciprocating pump, which by all accounts is the first documented instance where the principle of enacting forces to a fluid was achieved through mechanical motion [1]. This single invention provided the grounds for some of the great leaps in the civil architecture that humanity now benefits from today. Of these leaps, many different designs of pumping devices have been created, one of which is an axial flow pump. The particles of working fluid in an axial flow pump do not change radial position as it is accelerated. While most axial flow pumps are used for civil purposes, axial flow pumps can be used as a means of naval propulsion. Pumps designed for the sake of propulsion are called waterjets and are generally powered by gas turbine engines, and it is of high interest to modern waterjet designers to optimize their performance.

In recent years, this task has evolved into understanding the fluid dynamics of the turbulent flows within waterjets. Almost all waterjets operate at high fluid velocities, which are no longer in the laminar class of flow. Currently, three different methods of modeling turbulent flow exist: Direct Numerical Solution (DNS), Large Eddy or Detached Eddy Simulation (LES/DES), and Reynolds-Averaged Navier Stokes (RANS). DNS resolves all turbulence and is the most computationally expensive, while LES resolves the large-scale eddies and models the turbulence scales below the grid resolution. RANS models all turbulence features, leading to significant reduction in computational cost. Therefore, it is still the most popular choice for simulating challenging flows around propellers and waterjets. This study focused on Unsteady RANS (URANS), which is the RANS model applied to transient flows.

This study adopts the URANS model from a commercial package SimericsMP+ to predict flow

features at high Reynolds numbers with rotating geometries. The URANS model will be first validated against CRP data and then applied to a naval waterjet. URANS involves separating the variables of interest such as instantaneous velocity into a steady, averaged part and a fluctuating part, as seen in Eq (1).

$$u = \bar{u} + u' \tag{1}$$

When this change is applied to the continuity and momentum equations, they take the form seen in Equation (2) and Equation (3). This leads to the formation of a new unknown term in the momentum equation $\rho \overline{u'_1 u_1}'$, called the Reynolds stress.

$$\frac{\partial \rho}{\partial t} + \frac{\partial}{\partial x_i} (\rho \overline{u_i}) = 0 \tag{2}$$

$$\frac{\partial}{\partial t}(\rho \overline{u}) + \frac{\partial}{\partial x_j}(\rho \overline{u_l} \overline{u_j}) = -\frac{\partial}{\partial x_j}(\rho \overline{u_l} \overline{u_j}) + \frac{\partial}{\partial x_j}\mu \left(\frac{\partial \overline{u_l}}{\partial x_j} + \frac{\partial \overline{u_j}}{\partial x_i}\right) - \frac{\partial P}{\partial x_l}$$
(3)

Several different methods have been developed to handle the Reynolds stress. These methods vary in the number of equations required to close the model, with Spalart-Almaras incorporating one additional equation, and models such as $k-\varepsilon$ and $k-\omega$ incorporating two. Due to the rapidly strained flows induced by CRPs and waterjets, the Renormalization Group technique is applied to the standard $k-\varepsilon$ model, as this models handling of the Reynolds stress has proven successful at handling these types of flows [2]. The transport equations of the RNG $k-\varepsilon$ model are seen in Equation (4) and Equation (5).

$$\frac{\partial}{\partial t}(\rho k) + \frac{\partial}{\partial x_i}(\rho \overline{u_j} k) = \frac{\partial}{\partial x_i}(\alpha_k \mu_{eff} \frac{\partial k}{\partial x_i}) + G_k + G_b + \rho \epsilon - Y_m + S_k \tag{4}$$

$$\frac{\partial}{\partial t}(\rho\epsilon) + \frac{\partial}{\partial x_i}(\rho\overline{u}_j\epsilon) = \frac{\partial}{\partial x_i}\left(\alpha_k\mu_{eff}\frac{\partial\epsilon}{\partial x_i}\right) + C_{1\epsilon}(G_k + C_{3\epsilon}G_b) - C_{2\epsilon}\rho\frac{\epsilon^2}{k} - R_{\epsilon} + S_{\epsilon}$$
 (5)

2. Validation Using CRP6

To ensure that the selected URANS method is able to analyze such complicated flow fields, simulations of DTMB CRP6 are used to validate the URANS solver before it is applied to AxWJ-2.

2.1 Geometry

Having been around for nearly four decades, the DTMB CRP6 has been subjected to rigorous experimental testing [3]. It's benchmark status made it a good candidate for validating the URANS solver. The set consists of two four-bladed propellers axially spaced 1.7 inches (0.28R) apart. Following the procedure laid out by Miller [3], both propellers are rotated at 12 revolutions per second while inlet speeds are varied. The main geometric parameters of the CRP set are listed below in Table 1. In Table 1, P is the pitch of the propeller, D is the diameter of each respective propeller, and A is the ratio of the part with even load distribution accounting for the whole chord length.

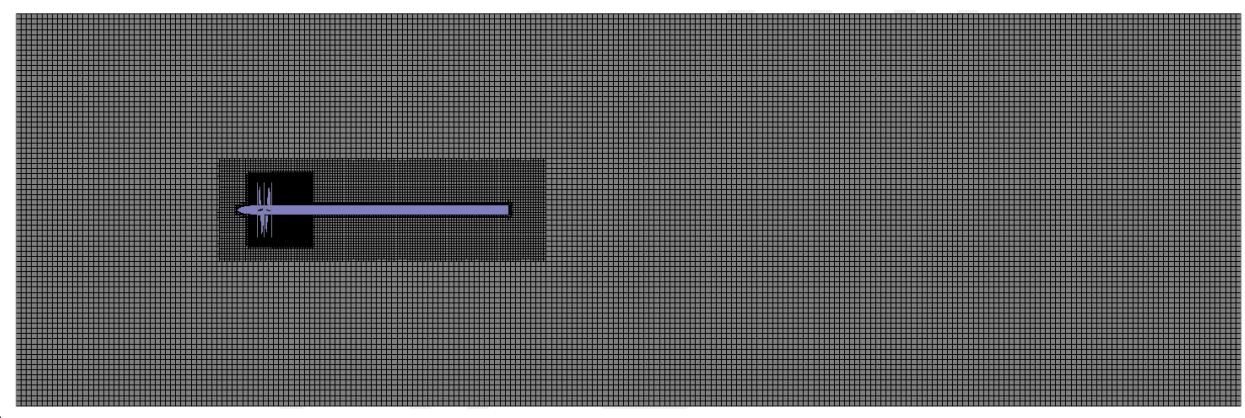
rable if the comment arameters		
	P3686	P3687A
Diameter (m)	0.3052	0.2991
Number of blades	4	4
$P_{0.7R}/D$	1.291	1.326
Expanded area ratio	0.303	0.324
Section camber and thickness	NACA66mod/a=0.8	NACA66mod/a=0.8
Direction of Rotation	CCW	CW
Position	Forward	Aft

Table 1: CRP6 Geometric Parameters

2.2 Computational Domain

The simulation domain is set up as a cylinder with a streamwise length of 25D and radius of 8D. The forward propeller is located 5D into the domain with a shaft that extends 5D downstream. Around the propellers, two cylindrical rotating meshes are used. On the surface of the propellers the cells have a size of approximately 0.5 mm, which grow to 2 mm for the rest of the rotating mesh. This element size

is set to ensure a y+ value of 60, which closely matches the value suggested by Wang and Xiong (2012) [4]. The rotating meshes have a diameter of 1.1D and a length of 0.15D. The elements in the stationary mesh are 32 mm in size. Three cylindrical refinement zones are created to better resolve the flow field surrounding the rotating meshes. The first zone starts 0.8D upstream of the forward propeller and has a length of 6.5D with diameter 2D. The cell size in this refinement zone is set to 16 mm. The second zone begins 0.25D upstream of the forward propeller with a length of 1.3D and diameter 1.44D. The final refinement zone is placed 0.125D upstream of the forward propeller, extending downstream just 0.4D with a diameter of 1.4D. The mesh used is illustrated in Figure 1. A total of 6,640,527 hexahedral elements are used, with the stationary mesh containing 3,612,869 elements and forward and aft rotating meshes containing 1,483,687 and 1,543,971 elements respectively. The inlet is set to free stream velocity, while the outlet is set to reference pressure. A slip wall boundary condition is used for the cylindrical walls. The shaft is modeled as a no-slip wall and a rotating no-slip wall is used on the propellers and hubs. At the design advance ratio, an additional simulation is run where the cell size in the rotating domains and first two refinement zones are halved, leading to a total cell count of 27,357,255, or about a 300% increase in cells in said region.



a)

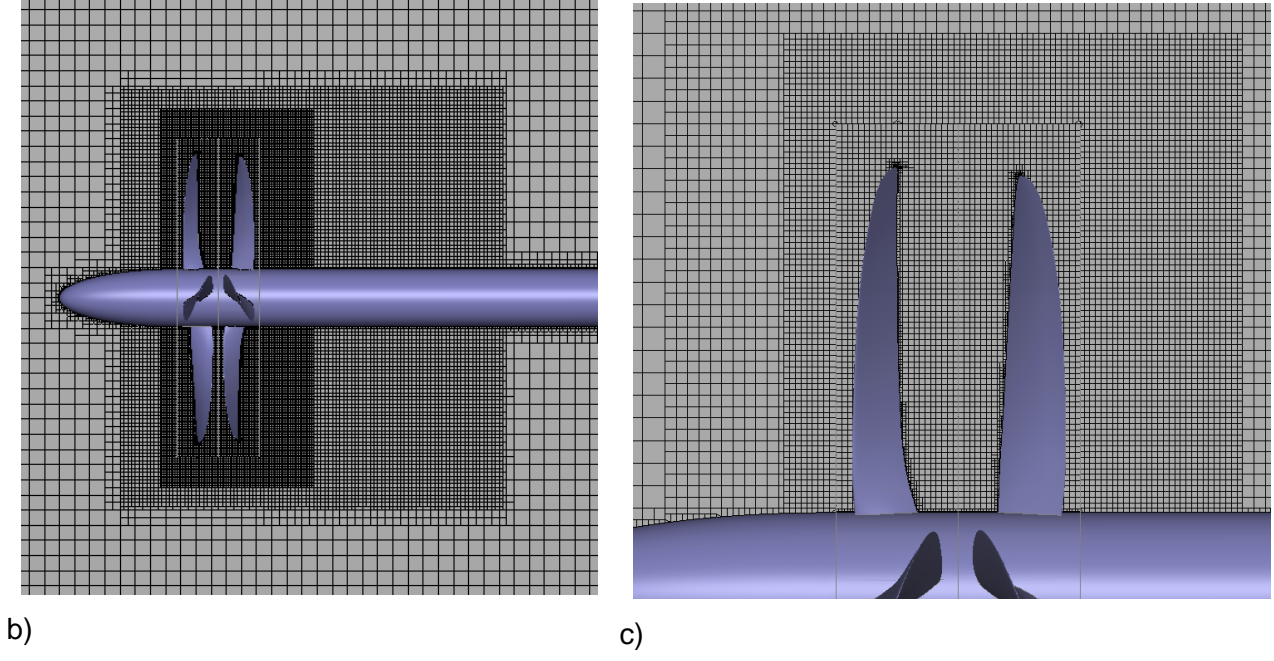


Figure 1 – Meshes used for DMT-CRP6 Simulation: a) complete domain b) refinement zones c) and close-up of rotating domains

2.3 Nondimensional Parameters

An important characteristic of fluid mechanics is the Reynolds number. In this case the Reynolds number is defined based on the chord length of the forward propeller at 0.7*R* as in Equation (6) To remain consistent with the experiment performed by Miller, conditions are matched such that simulations occurred at Reynolds numbers ranging from 510,000 to 580,000.

$$Re = \frac{c_{0.7R} \sqrt{U_{\infty}^2 + (0.7\pi nD)^2}}{v}$$
 (6)

An additional parameter is the advance ratio of the propeller defined in Equation (7), which relates the advancing speed to propeller spin rate.

$$J = \frac{U_{\infty}}{nD} \tag{7}$$

where n is the rotational speed of the propeller in rotations per second. The design operating conditions for the propeller are seen in Table 2

Table 2: CRP6 Design Conditions

Reynolds Number	5.49×10^{5}	
Free Stream Velocity (m/s)	4.03	
Kinematic Viscosity	8.917×10^{-7}	
Advance Ratio	1.1	

Two other nondimensional numbers are used to study the propeller mechanics – the thrust coefficient K_T and the torque coefficient K_Q defined in Equation (8) and Equation (9), respectively.

$$K_T = \frac{T}{\rho n^2 D^4} \tag{8}$$

$$K_Q = \frac{Q}{\rho n^2 D^5} \tag{9}$$

where ρ is the fluid density, T is the thrust produced by the propeller, and Q is the torque.

3. Application to ONR Waterjet AxWJ-2

Concluding the validation study with CRP6, the largest error in coefficient value remained under 10%. Thus confidence is placed in Simerics' ability to analyze complex rotational flows and simulations of the wateriet are performed.

3.1 Geometry

The axial flow water jet pump examined in this study was designed by Michael et al [5]. Figure 2 below demonstrates the geometry of the turbine. The rotor, designated rotor 5521, consists of six blades, while the stator (5522) consists of eight blades. AxWJ-2 was designed and built at several different model scales for performance testing at different water tunnel facilities. For this study, the 12" diameter model is used. This model varies from the larger scale models as it employes an enlarged spacing between the rotor and stator to allow for ease of experimental data collection. As this region is of no significance to this study, this spacing is made solid as to save computational resources. Another modification made to this model was the extension of the exit nozzle, which was done to produce a uniform pressure field across the exit plane for the sake of performing measurements. The effect of the stator, as well as the extension of the exit nozzle on performance is investigated.

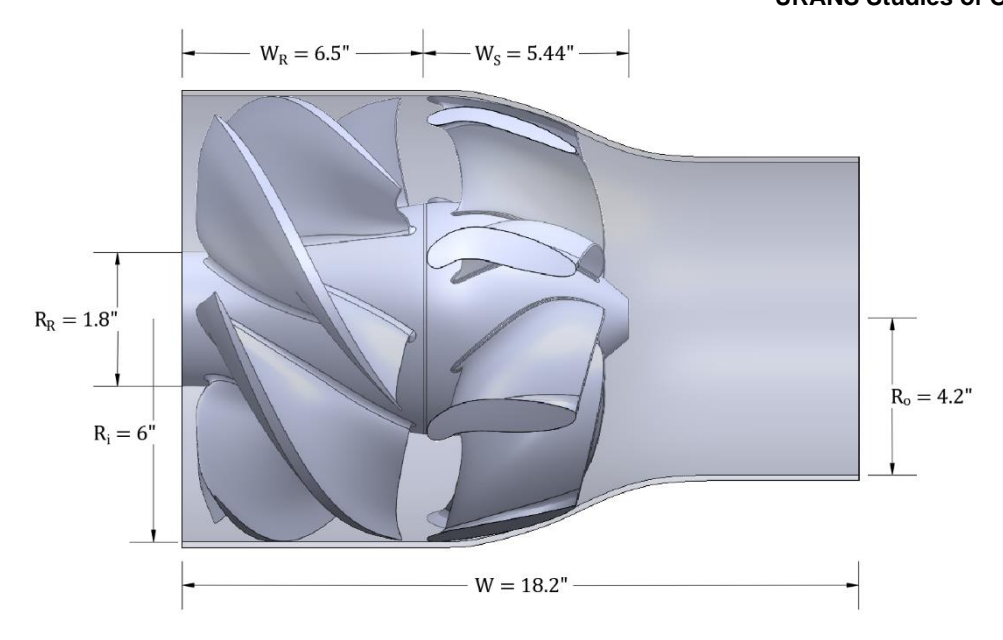


Figure 2 – Geometry of ONR Waterjet AxWJ-2

3.2 Computational Domain and Method

The fluid domain used in these simulations is bounded by the geometry of the casing and consists of two separate but connected regions. Both regions utilize an element size of 2 mm, which leads to a total of 3,823,690 elements. Figure 3 shows a section view of the computational mesh. A rotating mesh with a total of 1,840,911 elements is used around the rotor. The stationary mesh contains a total of 1,982,779 elements. On the surfaces of both the rotor and stator, cells have a size of 1 mm, which corresponds to a y+ value of 250. A no-slip wall condition is applied to the casing walls, as well as to the stator walls and hub. A rotating no-slip wall is used on the rotor. A prescribed volumetric flow rate is assigned to the inlet, and the outlet is modeled as a pressure outlet. At the design flow coefficient, an additional simulation is run where the cell size in both regions is halved, leading to a total cell count of 24,589,043 or about a 6.5x increase in cells. The mesh used can be seen below in Figure 3.

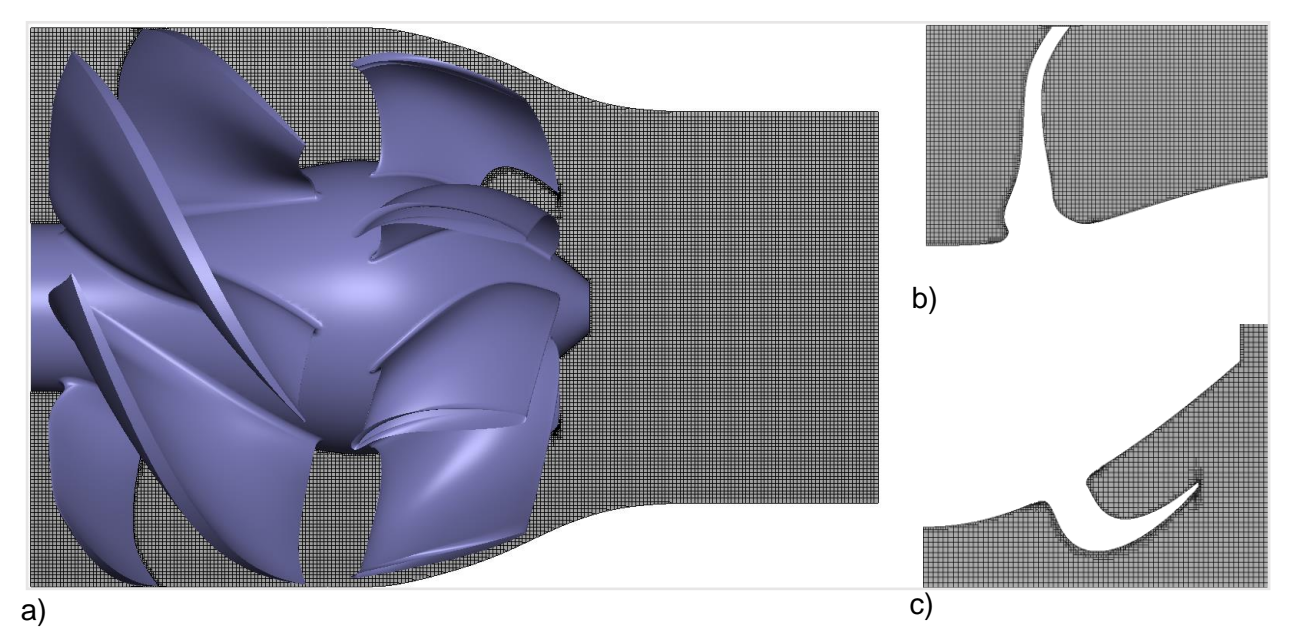


Figure 3 – Meshes used for ONR AxWJ-2 Simulation: a) complete domain b) close-up of rotor blade c) and close-up of stator blade

3.3 Nondimensional Parameters

The Reynolds number used to study the water jet is defined slightly different from the propeller as the characteristic speed and length is based on rotor tip speed and chord length. The second important nondimensional parameter is the flow coefficient, which is defined in Equation (10). Like the advance ratio, the flow coefficient relates the advancing (inlet) speed with the rotational speed of the rotor. This paper examined the effect of the flow coefficient on the performance of the water jet.

$$Q^* = \frac{\dot{\mathbf{v}}}{nD^3} \tag{10}$$

Where $\dot{\forall}$ is the volumetric flow rate of the waterjet in cubic meters per second. The design operating conditions for the waterjet are seen in Table 3.

Table 3: CRP6 Design Conditions

Reynolds Number	1.25×10^{6}
Flow Coefficient	0.85
Kinematic Viscosity	1.466×10^{-5}
n (rpm)	2000

Nondimensional head and torque coefficients are calculated at these conditions, and then used to study the effect of varying Q^* . They are defined in Equation (9) and Equation (11), respectively.

$$H^* = \frac{\Delta P}{\rho(nD)^2} \tag{11}$$

Where ΔP is the pressure change between the inlet and outlet of the waterjet.

4. Results

For all simulations, time-step size selection is based on the recommendation of Wang and Xiong [4], who investigated the roles timestep size and turbulence model play in producing reasonable URANS results for CRPs. For both CRP and waterjet simulations, a timestep size which corresponded to one time-step per degree of rotation is used. For all simulations, a second-order upwind differencing scheme is used to solve the momentum equations, as well as for time. Turbulence closure equations are solved via a single order differencing scheme. Due to the large element count and number of timesteps, all simulations are performed across 80 parallel computer cores, each taking roughly 6 hours to complete.

4.1 CRP6

The simulation for CRP6 is stopped once the thrust and torque coefficients clearly converged. In this case, both reached an oscillatory stage where they fluctuated within a percentage of an average value. This can be seen in the results at the design advance ratio in Figure 4 which displays these oscillatory fluctuations over one rotation. Notably, when both propellers are rotated by 45°, the thrust and torque of each propeller repeat leading to 8 peaks per revolution. The amplitude of the forward propeller fluctuations is about 40% of the average, which is almost four times larger than the 12% fluctuation amplitude of the aft propeller.

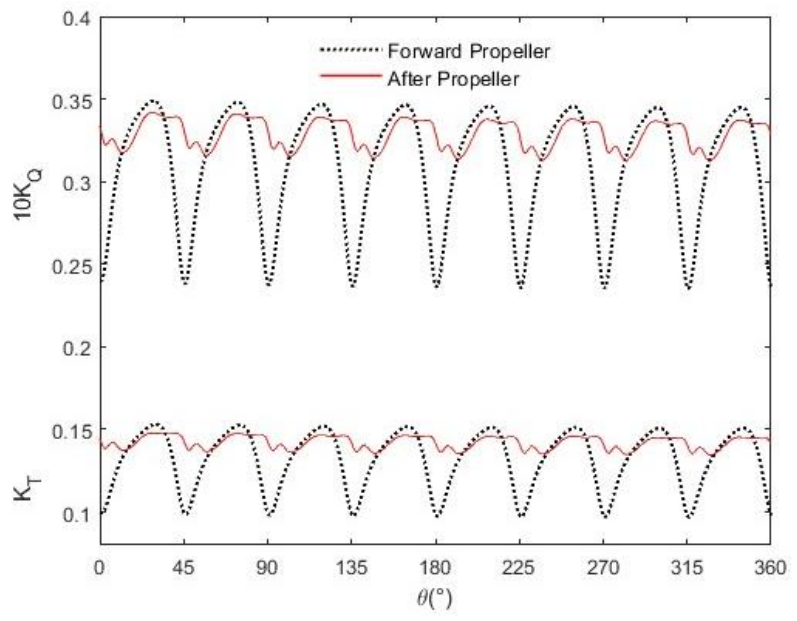


Figure $4 - K_T$ and $10K_Q$ as a function of rotation

From these results, the time-averaged values for K_T and K_Q on the forward propeller are found to be 0.1302 and 0.0305 respectively, and 0.1398 and 0.0325 on the aft propeller. These values are all within 10% of the experimental data collected by Miller. Simulations with the finer mesh produced slightly closer values but did not show a significant change. As it is now apparent that URANS can deal with complicated rotational fields, simulations are run over a range of advance ratios and compared to empirical data. The results of this study can be seen in Figure 5 below. Across all advance ratios, it is concluded that the forward propeller is responsible for producing roughly 46% of the total thrust, while the aft produces the remaining 54%. This effect is most likely caused by the induced wake on the aft propeller created by the forward.

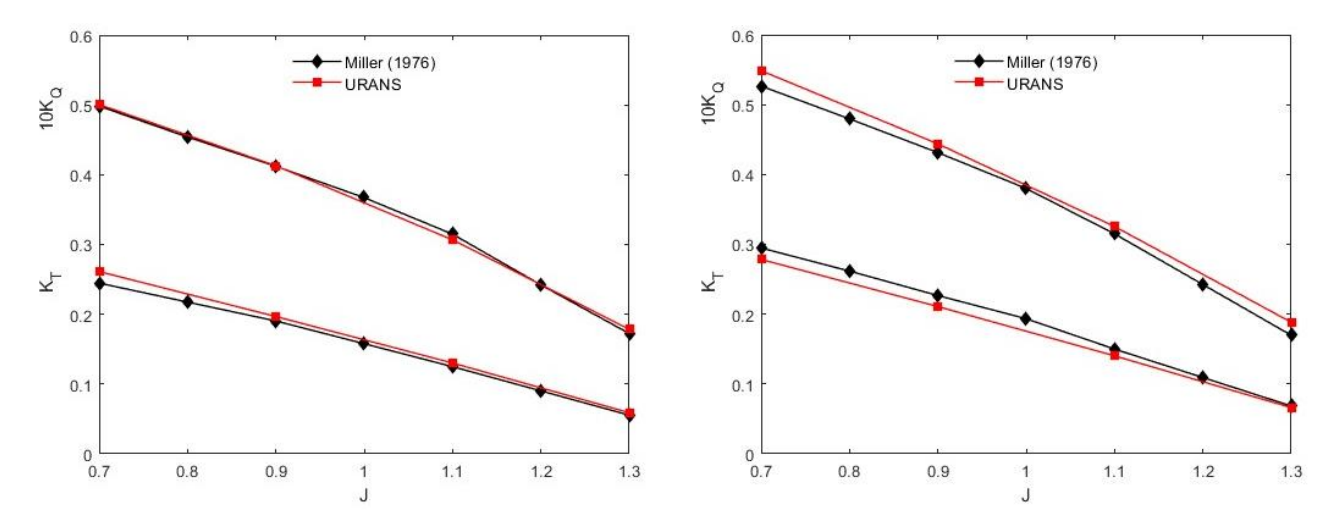


Figure 5 – K_T and 10K_Q as a function of advance ratio for forward (left) and aft (right) propellers

4.2 ONR Waterjet AxWJ-2

Similar to CRP6, the values of torque and head began to oscillate about a mean value, however these fluctuations occurred at a much smaller amplitude. The amplitude of the head is about 1.5% of the average, while the fluctuation amplitude of the torque is less than 1%. Following the procedure used for CRP6, time averaged values are taken for K_Q and H^* after their apparent convergence. The time-averaged value for H^* is found to be 2.23 while K_Q is found to be 0.341. These values are both less than 2% different than the experimental data collected by Michael. The results of this simulation can be seen in Figure 6. The finer mesh had slightly closer values but did not show a significant change.

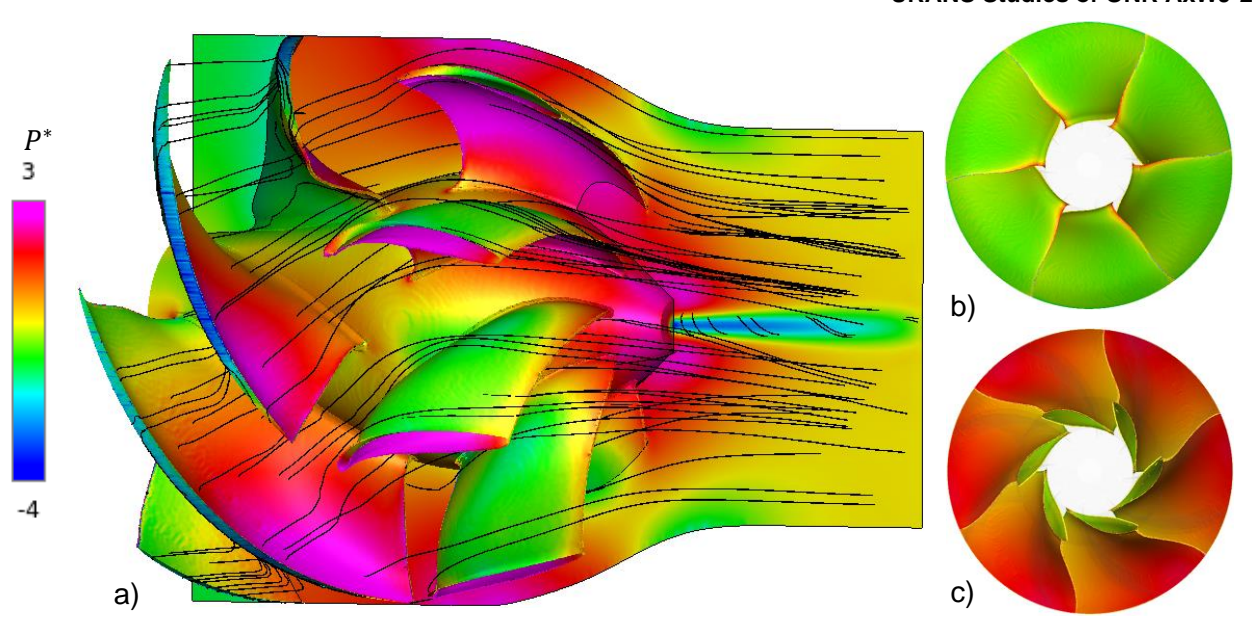


Figure 6 – Normalized pressure distribution for a) entire waterjet b) rotor suction side c) rotor pressure side

Figure 6 above displays the working principle of waterjets. Probe points are used to collect pressure values upstream and downstream of the rotor blade row. As the rotor rotates, the average downstream total pressure just past the rotor increases by a factor of 20, causing more fluid to be pulled into the rotor. The gap between the rotor blade and casing wall must be small as to maximize the amount of work done by the rotor. This gap leads to a pressure between the tips and casing wall 180 times greater than freestream. This action accelerates the flow from 11 to 21 m/s, inducing over 1100 N-m of torque on the stator as it is redirected. During this redirection the casing reduces in size by a factor of 1.4, further accelerating the flow to an exit velocity of 22 m/s.

It is of interest to determine the role the stator and extended nozzle plays in waterjet performance. Thus, simulations occurred excluding these elements. For this study, meshing and simulation settings are kept consistent with the full geometry study, and simulations are run at the design flow coefficient. At the design flow coefficient, the extension of the exit nozzle plays little role in waterjet performance as its removal only lead to a 2% increase in normalized head. This minor change was to be expected, as the nozzle was extended purely to ensure a uniform pressure distribution for ease of experimental data acquisition – a task it is successful at. However, removing the stator led to a drastic drop in waterjet performance. At the design flow coefficient, it is concluded that the waterjet produces 20% less of a pressure change when the stator is removed. This indicates the magnitude of the role the stator plays in performance, as without the axial redirection of the swirling fluid much of the imparted energy is wasted. This redirection is demonstrated in Figure 7 below.

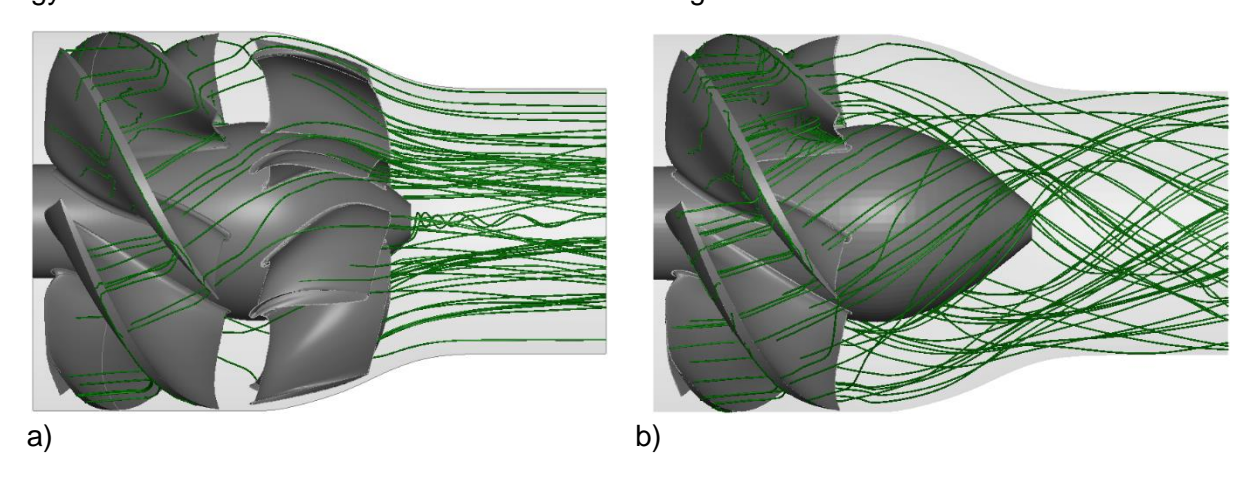


Figure 7 – Streamlines comparison a) with stator b) without stator

As it is unlikely that the waterjet will always operate at the design flow coefficient, it is of interest to determine the performance characteristics at different flow conditions as well as examine the causes for loss in performance. Thus, simulations at different flow conditions are run and the coefficient averaging procedure mentioned above is repeated. Figure 9 below shows the velocity contours at different flow coefficients. From Figure 9 it is evident that at flow coefficients below design, the fluid swirls excessively, which leads to a drop in applied torque and decrease in efficiency. At flow coefficients above design, the blades fail to spin fast enough to effectively do work to the fluid which corresponds to a drop in both applied torque and head and in turn, efficiency. These trends are summarized in Figure 8, where it is clear that a maximum applied torque is achieved very close to the design flow coefficient, 0.85, confirming that AxWJ-2 is well designed.

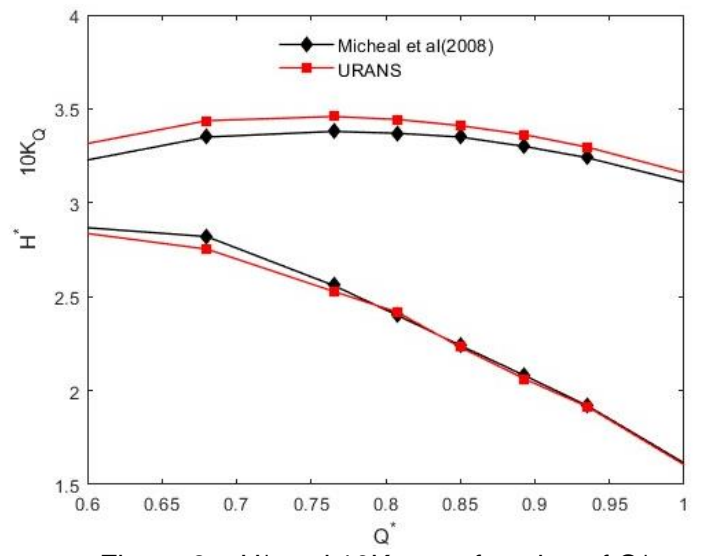


Figure 8 – H* and 10K_Q as a function of Q*

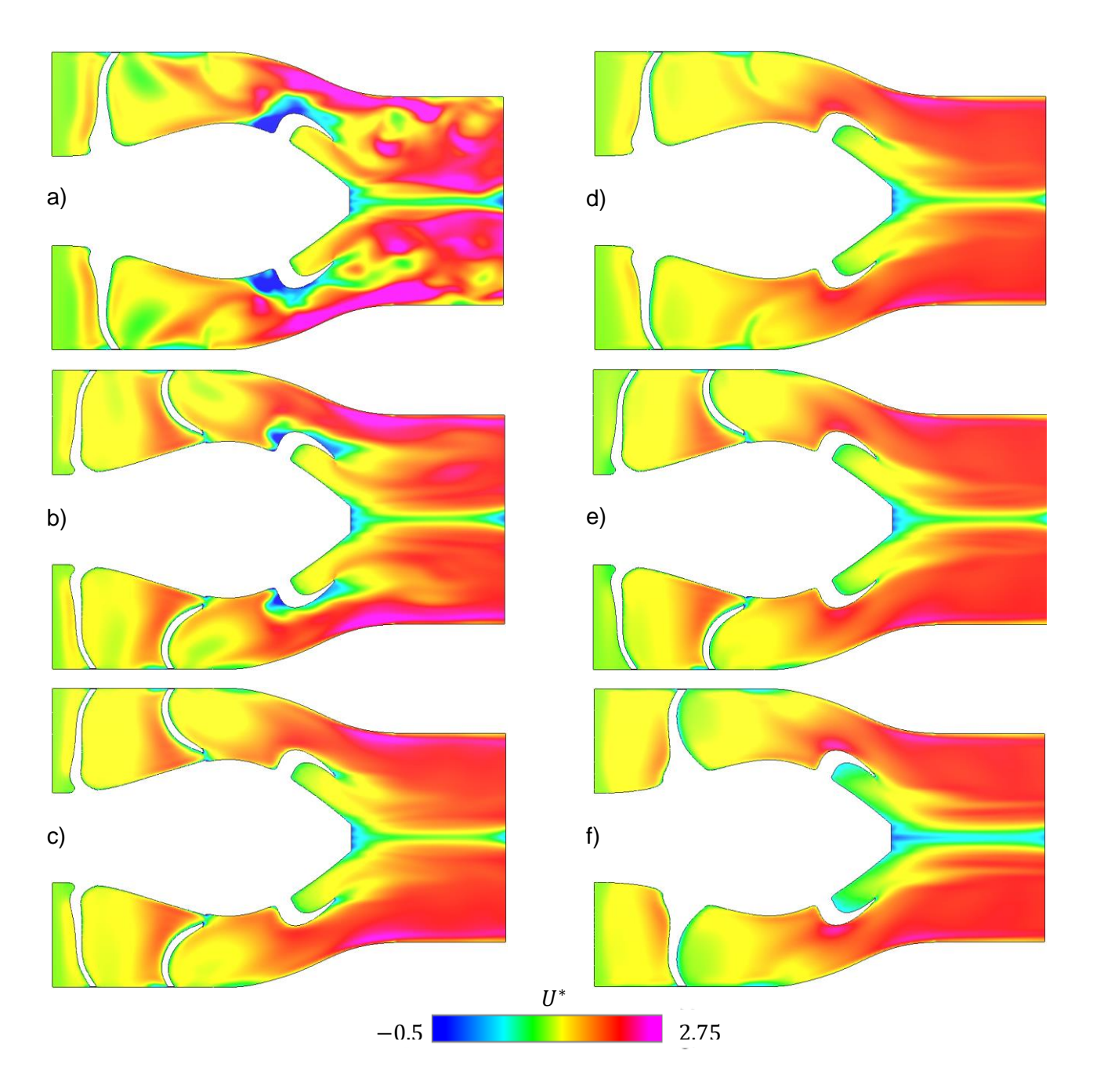


Figure 9 – Velocity Contours of AxWJ-2 with Q* = a) 0.595 b) 0.680 c) 0.765 d) 0.85^* e) 0.935 f) 1.02

5. Conclusion

The URANS model is a fast and reasonably accurate way to study turbulent flows involving rotating geometries. The Simerics software used was able to resolve complicated geometries and generate high-fidelity results within days using a moderate number of computer processors. URANS was able to predict torque and thrust coefficients for the DMTB CRP6 marine propeller set within 10% difference from the experimental data and reproduced numerical results for AxWJ-2 within 3%. This speed and accuracy make URANS a useful tool to study the fluid dynamics of a waterjet. One quantitative takeaway from this study is the revealed importance of the stator. Without the redirection of the bulk flow back into the axial direction by the stator, the waterjet produces nearly 20% less power, a significant amount. This redirection by the stator is of the same ideology of incorporating a counterrotating propeller to a conventional propeller system, but the effect the stator induces is much larger. It can also be concluded that AxWJ-2 is very well designed, as it achieves maximum torque and efficiency at the design conditions.

6. Acknowledgements

I would like to thank Dr. Chunlei Liang of the Mechanical and Aerospace Engineering Department for his assistance with preparing my MS Thesis. I am also grateful for the graduate assistantships awarded by the MAE department, as well as the NSF High Performance Computing (HPC) REU hosted by Drs. Daqing Hou and Yu Liu of the Electrical and Computer Engineering Department with award no. 1852102. I am also very grateful to Dr. Junfeng Wang from Simerics for helping me learn the software. All computations were performed using the ACRES computer cluster at Clarkson University.

7. Contact Author Email Address

For any questions regarding this work, please mailto: stephen.monroe9@gmail.com

8. Copyright Statement

The author confirms that they, and Clarkson University, hold copyright on all of the original material included in this paper. The author also confirms that they have obtained permission, from the copyright holder of any third-party material included in this paper, to publish it as part of their paper. The author confirms that they give permission or have obtained permission from the copyright holder of this paper, for the publication and distribution of this paper as part of the ICAS proceedings or as individual off-prints from the proceedings.

References

- [1] The History of Pumps: Through the Years (2011) Pumps and Systems Magazine. Available at: https://www.pumpsandsystems.com/history-pumps-through-years (Accessed: February 10, 2023).
- [2] Orszag, S. A., Yakhot, Flannery, W. S., Boysan, F.E., Choudhury, D., Maruzewski, J., & Patel, B., "Renormalization Group Modeling and Turbulence Simulations", *International Conference on Near-Wall Turbulent Flows*, Tempe., 1993
- [3] Miller, M.L., "Experimental Determination of Unsteady Forces on Contrarotating Propellers in Uniform Flow," David Taylor Research and Development Center Report Number 659-01, 1976
- [4] Wang, Z. and Xiong, Y., "Effect of Time Step Size and Turbulence Model on the Open Water Hydrodynamic Performance Prediction of Contra-Rotating Propellers", Chinese Ocean Engineering, 2012 Vol 27, No. 2, pp. 193-204
- [5] Michael, T. J., Schroeder, S. D., and Becnel, A. J., "Design of the ONR AxWJ-2 Axial Flow Water Jet Pump," NSWCCD-50-TR-2008/066, November, 2008.
- [6] Jessup, S., Donnelly, M., Fry, D., Cusanelli, D., and Wilson, M., "Performance Analysis of a Four Waterjet Propulsion System for a Large Sealift Ship," 27th Symposium on Naval Hydrodynamics, Seoul, Korea, October 5-10 2008.
- [7] Chesnakas, C. J., Donnelly, M. J., Pfitsch, D. W., Becnel, A. J., and Schroeder, S. D., "Performance Evaluation of the ONR Axial Waterjet2 (AxWJ-2)," NSWCCD-50-TR-2009/089, December, 2009